Water adsorption behaviour on (001) pyrophyllite surface from ab initio Density Functional Theory simulations

#Post-print of the article published in Applied Clay Science, 2021, 212, 106221, DOI https://doi.org/10.1016/j.clay.2021.106221

Water adsorption behaviour on (001) pyrophyllite surface from a*b initio* Density Functional Theory simulations

Gianfranco Ulian[1], Daniele Moro[1], Giovanni Valdrè[1*]

[1]*Centro di Ricerca Interdisciplinare di Biomineralogia, Cristallografia e Biomateriali, Dipartimento di Scienze Biologiche, Geologiche e Ambientali, Università di Bologna "Alma Mater Studiorum", Piazza di Porta San Donato 1, 40126 Bologna, Italy*

* Giovanni Valdrè, giovanni.valdre@unibo.it, ORCID 0000-0003-4280-2186

Abstract

The present study focuses on the interaction between water and a single layer of the (001) pyrophyllite surface. Pyrophyllite [$Al_2Si_4O_{10}(OH)_2$] is an important phyllosilicate characterized by strong in-plane covalent bonds and weak van der Waals interactions holding the structural layers together. The investigation was carried out by *ab initio* Density Functional Theory simulations, performed both at 0 K and room conditions (300 K, 1 bar) using static and molecular dynamics approaches, respectively. The adsorption of one to three water molecules, investigated by static method, showed that the hydration is completely driven by van der Waals interactions and, as the water content increases, so does the tendency of the solvent to self-assemble. In fact, the binding energies per H_2O molecule were calculated as -17.2 kJ mol^{-1}, -11.8 kJ mol^{-1}, and -11.6 kJ mol^{-1} for the adsorption of one, two, and three water molecules, respectively. The results showed that water forms structures that resemble those typically found in the gas phase, *i.e.* water dimer and triangular cluster. Regarding the latter, the *ab initio* molecular dynamics simulations proved that this self-assembly is stable over the considered time for the run. These findings are in good agreement with the few previous data reported in the literature and could be of great use for both experimental and theoretical applications in both mineralogy and petrography and for the development of bidimensional van der Waals material from natural sources.

Keywords: *Layered silicates; van der Waals layered materials; pyrophyllite; (001) surface; water adsorption; Density Functional Theory*

1. Introduction

Pyrophyllite is a dioctahedral phyllosilicate whose ideal chemical formula is $Al_2Si_4O_{10}(OH)_2$. According to the experimental characterization of Evans and Guggenheim (1988), this mineral exists in three polymorphs, *i.e.* monoclinic (2*M*), triclinic (1*Tc*), and disordered. Figure 1 reports the structure of 1*Tc* polymorph, where each layer of the mineral is composed of tetrahedral (T) and octahedral (O) sheets in a 2:1 ratio (T-O-T, or TOT structure). The T sheet is formed by single SiO_4 tetrahedra that share three oxygen atoms [basal oxygen, O(b)] with other SiO_4, resulting in an

infinite 2D sheet with a hexagonal-like pattern. The fourth vertex of the silica tetrahedron [apical oxygen, O(a)] is shared with the octahedrally-coordinated cations (usually aluminium). Within this O sheet, the individual octahedra are linked by edge sharing and only 2/3 of the octahedral sites are occupied (dioctahedral phyllosilicate). According to the stoichiometry of the mineral, the TOT layers are electrically neutral and only weak van der Waals interactions hold them together along the stacking direction. This specific crystal-chemistry explains both the extreme softness of the mineral along [001] direction and the exfoliation occurring perpendicularly to the crystallographic *z*-axis (Ulian and Valdrè, 2015c).

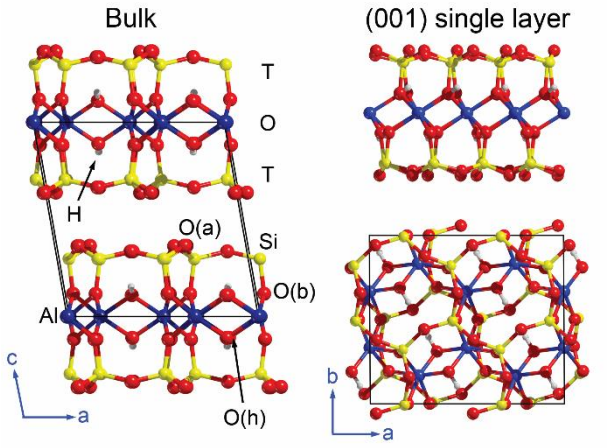

Figure 1. (left panel) Bulk structure of pyrophyllite 1*Tc*. (right panel) Views along the [010] and [001] directions of the (001) surface model of pyrophyllite (PYP). The black lines show the 2D unit cell of the slab. Colour code for atoms: Si – yellow, Al – blue, O – red, H – white. O(b), O(a), and O(h) are basal, apical, and hydroxyl oxygen atoms, respectively.

From the mineralogical and geological points of view, pyrophyllite has an important role as a hydrous phase because it contains several hydroxyl groups, hence it can recycle water into the Earth's mantle via processes occurring in the subduction zone (Pawley et al., 2002). Industrially, it is also employed in whiteware ceramics (Bhasin et al., 2003), petroleum and civil engineering, food and cosmetics, and waste storage (Ulian and Valdrè, 2015c). Furthermore, pyrophyllite can be considered as a prototype for the description of the hydration of clay minerals. In contrast with defective phases such as smectites (expandable clays), which present several isomorphic substitutions in different crystallographic sites, the electrical neutrality of the stoichiometric TOT layer makes the (001) surface of pyrophyllite hydrophobic (Bridgeman et al., 1996; Churakov, 2006).

Because of its peculiar crystal chemistry, pyrophyllite could be also a potentially interesting substrate for the realization of van der Waals heterostructures with either conductive or semi-

conducting single-layered materials. In fact, the experimental discovery of graphene in the first years of the XXI century (Novoselov et al., 2004) opened new researches and application of the so-called two-dimensional materials. Since then, many efforts were devoted to advance the fundamental and practical knowledge of these innovative materials, which include hexagonal boron nitride (Pan et al., 2012), black phosphorene (Cheng et al., 2020), layered double hydroxides, molybdenite, and other transition metal dichalcogenides (Dong et al., 2018; Mak et al., 2010), and combination of them in *z*-stacked van der Waals heterostructures (*e.g.*, (Baranava et al., 2018; Ulian et al., 2021; Yang et al., 2018). An interesting fact about these 2D materials is that, in most cases, including graphene, their discovery began from high-purity natural sources, *i.e.* minerals. Indeed, there are several mineralogical phases exhibiting heterodesmic structures, namely strong covalent/ionic bonds within the *x*-*y* plane and weak long-range interactions along the *z*-direction. Among them, phyllosilicates are quite abundant in nature and present very interesting surface properties that could be potentially employed for catalysis (Moro et al., 2019b; Quaranta et al., 2021; Ulian et al., 2018; Valdrè et al., 2011).

In the context of both mineral-petrographical and catalytic applications and the development of nature-driven bidimensional van der Waals materials, the present work aims at obtaining a better comprehension of the hydration of pyrophyllite. Since this mineral does not exhibit swelling, namely no water molecule enters in the interlayer between TOT layers, in this study the adsorption involved the (001) surface of pyrophyllite. The investigation is conducted within the Density Functional Theory (DFT), employing both static (*i.e.*, carried out at 0 K) and *ab initio* molecular dynamics simulations at ambient conditions (300 K, 1 bar). Corrections for the weak dispersive forces were included in the physical treatment, because they are mandatory for this kind of system (Cutini et al., 2020; Ulian et al., 2013). The hydration process was simulated considering an increasing number of water molecules on the (001) mineral surface, from one to three. A similar approach was proposed in the relatively recent theoretical work of Zhang and co-workers (2012), where a combination of static and dynamic simulations was performed. However, while the 0 K characterization was conducted with a DFT approach using the VASP code, projector-augmented wave (PAW) basis sets, PBE functional and D2 dispersion correction, the time evolution dynamic of the (001) pyrophyllite hydration was investigated with molecular mechanics (force field) simulations. The novelty of the present paper resides in employing well-known hybrid DFT functionals for the static characterization and *ab initio* molecular dynamics (AIMD) simulations for the determination of the dynamic of the water/pyrophyllite interaction. This represents an improvement over the use of force field (*i.e.*, parametrized) methods.

2.Theoretical methods

2.1. Pyrophyllite (001) surface model

The single-layered (001) surface of pyrophyllite was realized as a slab that was cut from the mineral bulk structure [1*Tc* polymorph, space group $C\bar{1}$]. The 1*Tc* triclinic structure is characterized by the presence of a single TOT layer in the unit cell. The starting bulk geometry was taken from a previous work where the structure and thermo-mechanical properties of pyrophyllite were investigated in detail at the DFT level (Ulian and Valdrè, 2015c). To have a sufficiently large surface area for the adsorption simulations, the *a* lattice parameter of the (001) slab model was doubled, thus the final lateral dimensions (prior geometry optimization, *vide infra*) were *a* = 10.335 Å and *b* = 8.983 Å, with surface area 92.841 Å^2. Finally, the single TOT layer of pyrophyllite retains the inversion centre inherited from the space group of the bulk mineral, hence the surface belongs to the layer group $P\bar{1}$. The (001) slab model of the mineral was labelled as PYP (Figure 1), a nomenclature that was employed throughout the paper.

2.2. Computational framework

The investigation on the (001) surface of pyrophyllite was conducted at the Density Functional Theory level, considering both static conditions (0 K) and *ab initio* molecular dynamic (AIMD) at ambient temperature and pressure) using CRYSTAL17 (Dovesi et al., 2018) and QuantumATK (Smidstrup et al., 2020), respectively. Since the codes have their specific keywords and approaches, the employed computational parameters will be presented separately in the next two paragraphs.

2.2.1. Static simulations

Within the CRYSTAL code, the simulations were performed with the well-known hybrid functional B3LYP (Becke, 1993; Lee et al., 1988), including an *ad hoc* correction to take into account the effect of long-range interactions in the physical description of the system. This correction is based on the DFT-D2 method formulated by Grimme (2006):

$$E_{\text{DFT-D2}} = -s_6 \sum_{\mathbf{g}} \sum_{i \neq j} f_{\text{dump}}\left(R^6_{ij,\mathbf{g}}\right) \frac{C_6^i C_6^j}{R^6_{ij,\mathbf{g}}} \quad (1)$$

$$f_{\text{dump}} = \frac{1}{1+e^{-d\left(R_{ij,\mathbf{g}}/R_{\text{vdw}}-1\right)}} \quad (2)$$

where C_6^i is the dispersion coefficient of the atom *i*, s_6 is a scaling factor whose value is 1.05 for B3LYP, and $R_{ij,\mathbf{g}}$ is the interatomic distance between atom *i* in the reference cell and atom *j* in the neighboring cells at distance |**g**|. The dumping function f_{dump}, whose expression is reported in Eq.(2), is used to avoid double-counting at short range, and depends on the sum of atomic van der Waals radii R_{vdw}. The values of the different parameters employed in these simulations are those suggested by Civalleri and co-workers (2008), where the scaling factor was set to s_6 = 1.00 and the atomic parameters are modified as shown in Table 1.

Table 1. Atomic parameters for the modified DFT-D2 approach employed in the present work.

Atom	C_6	R_{vdw}
Si	9.23	1.8018
Al	10.79	1.8018
O	0.70	1.4091
H	0.14	1.3013

This approach is called B3LYP-D*, and was already successfully employed in the description of bulk pyrophyllite (Ulian and Valdrè, 2015c).

The exchange and correlation terms of the total energy are obtained through numerical integration of the electron density and its gradient, the operation performed on a large pruned grid (XLGRID keyword in CRSYAL, 75 radial points, and 974 angular points) (Dovesi et al., 2018). The Hamiltonian matrix was diagonalized using a shrinking factor of 2 (SHRINK keyword), meaning that it was employed a 2 × 2 × 1 Monkhorst-Pack (bidimensional) grid that considers 4 *k* points (Monkhorst and Pack, 1976). This is a reasonable choice between high accuracy and calculation speed. Total energy accuracy was set to 10^{-8} Ha via the TOLDEE keyword, whereas the truncation criteria for the bielectronic integrals were chosen as the default provided by CRYSTAL (TOLINTEG 7 7 7 7 14). Regarding the geometry optimization procedure, it was employed a scheme proposed by Schlegel (1982) that was adopted for both dry and hydrated pyrophyllite surfaces. The structural convergence is mainly controlled by two keywords, TOLDEG and TOLDEX, namely the thresholds of the root mean square on gradient and on the estimated displacements, respectively, which were set to $3.0 \cdot 10^{-4}$ au, and $12 \cdot 10^{-4}$ au (Dovesi et al., 2018).

The multielectronic wave function is constructed in the CRYSTAL code from a Linear Combination of Atomic Orbitals (LCAO). More precisely, each crystalline orbital is a linear combination of Bloch functions defined in terms of atomic orbitals, the latter being Gaussian-type

functions (GTF). The choice of the GTFs is made on those already employed with good results on both bulk and surface properties of phyllosilicates (Moro et al., 2019a; Moro et al., 2015; Moro et al., 2019b, 2020a; Ulian et al., 2018, 2020; Ulian et al., 2013; Ulian et al., 2014; Ulian and Valdrè, 2015a, b, c; Ulian and Valdrè, 2019). Throughout all the simulations, the atomic orbitals of Si, Al, O, and H were described by means of 88-31G* (Nada et al., 1996), 8-511d1G (Catti et al., 1994), 8-411d11G (Valenzano et al., 2006) and 3-1p1G (Gatti et al., 1994) basis sets, respectively.

The energy involved in the adsorption process, namely the binding energy E_B, is defined in the present work as the amount of energy released when the water molecule is adsorbed on the mineral substrate, according to a reaction of the type:

$$S + W \rightarrow SW ,$$

where S, W and SW indicate the slab, the water molecule and the slab-water system, respectively. From the energy perspective, this reaction is translated into:

$$E_B = E(SW//SW) - E(E//S) - E_M(W//W) \quad (3)$$

where the term E(SW//SW) represents the energy of the water/pyrophyllite system, E(*S*//*S*) is the energy of the sole (001) slab and E_M(W//W) is the molecular energy of the water molecule in gas phase. The label following the double slash indicates the geometry at which the energy terms were calculated: for instance, the energy E_M(W//W) was calculated for the water molecule optimized in the gas phase. As written in Eq. (3), when H_2O is physisorbed onto the layered mineral the binding energy value is negative (Chiatti et al., 2016; Corno et al., 2009; Moro et al., 2015; Moro et al., 2019b). To obtain more information on the adsorption process, it is more convenient to rewrite Eq.(3) as:

$$E_B = E_B^* - \delta E_S - \delta E_W = E_B^* - \delta E_S - \Delta E_W - \Delta E_L \quad (4)$$

where δE_S and δE_W are the deformation energy of the slab and of water, respectively, and *BE** is the binding energy without these two contributions. The E_B^* and deformation energies are defined as:

$$E_B^* = E(SW//SW) - E(S//SW) - E(W//SW) \quad (5)$$

$$\delta E_S = E(S//SW) - E(S//S) \quad (6)$$

$$\delta E_W = \Delta E_W + \Delta E_L = E(W//SW) - E_M(W//W) \quad (7)$$

In addition, it is possible to calculate the pure deformation of the adsorbant, ΔE_W, and the lateral interaction term, ΔE_L, *i.e.* the interaction energy between the water molecule and its replicas in neighbouring unit cells:

$$\Delta E_W = E_M(W//SW) - E_M(W//W) \quad (8)$$

$$\Delta E_L = E(W//SW) - E_M(W//SW) \quad (9)$$

where E_M(W//SW) is the molecular energy of water in the adsorbed geometry. The values resulting from Eq.(6) and Eq.(8) are always positive, whereas ΔE_L may be either positive (repulsion) or negative (attraction).

Binding energy calculated using the LCAO approach is always overestimated due to the basis set superposition error (BSSE). This term was here calculated with the counterpoise method proposed by Boys and Bernardi (Boys and Bernardi, 1970), whose definition is:

$$\mathrm{BSSE} = E_B - E_B^C \tag{10}$$

The $E_B{}^C$, namely the BSSE-free binding energy is obtained as:

$$E_B^C = E_B^{*C} - \delta E_S - \delta E_W = E_B^{*C} - \delta E_S - \Delta E_W - \Delta E_L^C \tag{11}$$

$$E_B^{*C} = E\left(\mathrm{SW//SW}\right) - E\left(\mathrm{S[W]//SW}\right) - E\left(\mathrm{[S]W//SW}\right) \tag{12}$$

In Eq.(12), the two terms E(S[W]//SW) and E([S]W//SW) represent the energy of the slab calculated with ghost functions on the water molecules and vice versa. When the simulation of the adsorption process involves multiple molecules, the Eqs.(8,9) must be modified as:

$$\Delta E_L^C = E\left(N \cdot \mathrm{W//SW}\right) - \sum_j \sum_{i(i \neq j)} E_M\left(\mathrm{W}_j[\mathrm{W}_i]//\mathrm{SW}\right) \tag{13}$$

$$\Delta E_W = \sum_j E_M\left(\mathrm{W}_j//\mathrm{SW}\right) - E_M\left(N \cdot \mathrm{W//SW}\right) \tag{14}$$

In fact, when there are N molecules, the lateral interaction energy between the adsorbate is also affected by BSSE. To avoid the consequent artificial increase of the binding energy between the surface and the water layer, the basis set superposition error in the ΔE_L must be considered as in Eq.(13) (Corno et al., 2009).

2.2.2 AIMD simulations

As previously introduced, *ab initio* molecular dynamics simulations were performed by means of the QuantumATK code (version Q-2019.12) (Smidstrup et al., 2020; Smidstrup et al., 2017). All the AIMD calculations were conducted within the Density Functional Theory framework, using an LCAO approach with numerical atomic orbitals basis sets with double-ζ quality plus polarization (DZP) (Fuchs and Scheffler, 1999). The chosen Hamiltonian was the standard PBE (Perdew et al., 1996), including the contribution of the dispersive force with the standard DFT-D2 scheme (Grimme, 2006). The sampling of the Brillouin zone was performed with a 2 × 2 × 1 Monkhorst-Pack mesh of k points. The molecular dynamic was calculated starting with two equilibration periods of 1 ps (time step of 1 fs): the first one was performed at 300 K using an *NVT* Nose-Hoover thermostat (Martyna et al., 1992) (time scale of 100 fs), whereas the second one employed the *NPT*

Martyna-Tobias-Klein thermo-barostat (Martyna et al., 1994), at 300 K and 1 bar. After these mandatory equilibration steps, the production simulation was performed using the *NPT* ensemble at 300 K and 1 bar of pressure for 5 ps (5000 steps of 1 fs). Even if the considered time scale of the production run was comparatively small to typical molecular mechanics simulations, it ensured enough time to describe the mean behaviour of the three water molecules on the (001) pyrophyllite surface.

3. Results and discussion

3.1. Structural features of single layer (001) pyrophyllite

The optimized (001) slab model of pyrophyllite is graphically shown in Figure 1. Lattice parameters and internal geometry (bond lengths and angles) are instead reported in Table 2. From the structural/mineralogical point of view, the oxygen atoms within layered silicates are subdivided as basal O(b), apical O(a), and hydroxyl O(h).

The lattice parameters *a*, *b* and γ and the internal geometry (bond lengths and angles) of the (001) surface of pyrophyllite are in good agreement with those of the mineral bulk, obtained from previous experimental measurements and theoretical simulations (Lee and Guggenheim, 1981; Ulian and Valdrè, 2015c). The lattice parameters are in line with the ones obtained by Churakov (2006) at the PBE level without correction for long-range interactions (a = 5.219 Å, b = 9.033 Å), which were not available at that time, and by Kwon and Newton (2016) using a PBE-D2 approach (a = 5.320 Å, b = 8.963 Å). Mean bond lengths calculated for the single layer PYP agree well with those of the external TOT layer of the surface model characterized by Bruno and co-workers (2006) at the Hartree-Fock level of theory with the CRYSTAL code. It is worth noting that in the cited work the bidimensional lattice parameters were kept fixed at the experimental values during the simulations. In general, the proposed approach is fine for the physical and chemical description of the considered layered system. In particular, the internal geometries of the PYP are consistent with those of the massive mineral, meaning that the surface reconstruction is almost negligible. Hence, as also stated elsewhere (Moro et al., 2015; Moro et al., 2019b, 2020a, b), considering a single layer of 2:1 phyllosilicate is sufficient for the treatment and analysis of surface adsorption phenomena.

Table 2. Lattice parameters *a*, *b* (in Å) and γ (in degrees) and internal geometry (bond lengths and angles) of the (001) slab model of pyrophyllite used in the present work: lattice parameters, surface area (in $Å^2$), mean bond lengths (in Å)

and angles (in degrees). Previous theoretical and experimental (single-crystal X-ray diffraction, sc-XRD) results on bulk pyrophyllite are reported for the sake of comparison.

	Present work	**Bulk B3LYP-D*** [a,†]	**Bulk PBE-D** [b,†]	**Bulk sc-XRD** [c,†]
a	10.3296	10.336	10.334	10.320
b	8.9713	8.956	8.978	8.966
c	-	9.317	9.300	9.347
γ	90.27	89.97	89.73	89.64
Area	92.669	-	-	-
Si – O(b)	1.6233	1.6236	1.628	1.617
Si – O(a)	1.6476	1.6461	1.648	1.632
Al – O(a)	1.9298	1.9290	1.923	1.924
Al – O(h)	1.8921	1.8938	1.894	1.889
O(h) – H	0.9583	0.9582	0.9710	-
O(b) – Si – O(b)	109.54	-	-	109.55
O(a) – Si – O(b)	109.40	-	-	109.28
O(a) – Al – O(a)	78.10	-	-	77.85
	94.50	-	-	94.76
	165.28	-	-	-
O(a) – Al – O(h)	94.71	-	-	95.15
	166.52	-	-	-
O(h) – Al – O(h)	76.88	-	-	76.52

a - Ulian and Valdrè (2015c)
b - Tunega et al. (2012)
c - Lee and Guggenheim (1981)
†The *a* lattice parameter was doubled to ease the comparison with the present results.

Figure 2 reports the electrostatic surface potential (ESP) of pyrophyllite, whose pattern is regular, with positive regions above the silicon atoms and the negative ones on both the basal oxygen atoms and the hydroxyl oxygen atoms. The potential is symmetric with respect to a mirror plane passing through the hydroxyl groups. According to the electrostatic surface potential features and considering a single siloxane ring, four O(b) atoms are placed in sites with only slightly negative because of the screening effect of the Si neighbouring atoms, and two basal oxygen (those on the mirror plane) are instead on positive electrostatic surface potential sites. These three-dimensional features are in excellent agreement with the electrostatic potential map calculated at 2 Å from the (001) surface by Bruno et al. (2006), and with the electrostatic surface potential maps obtained by Churakov (2006) at different heights from the basal oxygen atoms. However, it is interesting noting several differences with respect to the electrostatic surface potential recently reported for talc, the trioctahedral analogue of neutral 2:1 phyllosilicates (Moro et al., 2020a). First, the pattern is very different, as there is not a clear hexagonal pattern of positive electrostatic surface potential on the silicon atoms and the tetrahedral ring centre is negative rather than positive. This is due to the O(h) – H bond being not perpendicular to the 2:1 layer, but slightly canted, with the oxygen atom exposed. Secondly, the ESP maximum value, in absolute terms, is two times that of talc. Hence, it

could be expected a different behaviour of the (001) pyrophyllite surface towards adsorption of water with respect to that observed for the (001) single layer of talc by Moro and co-workers (2020a).

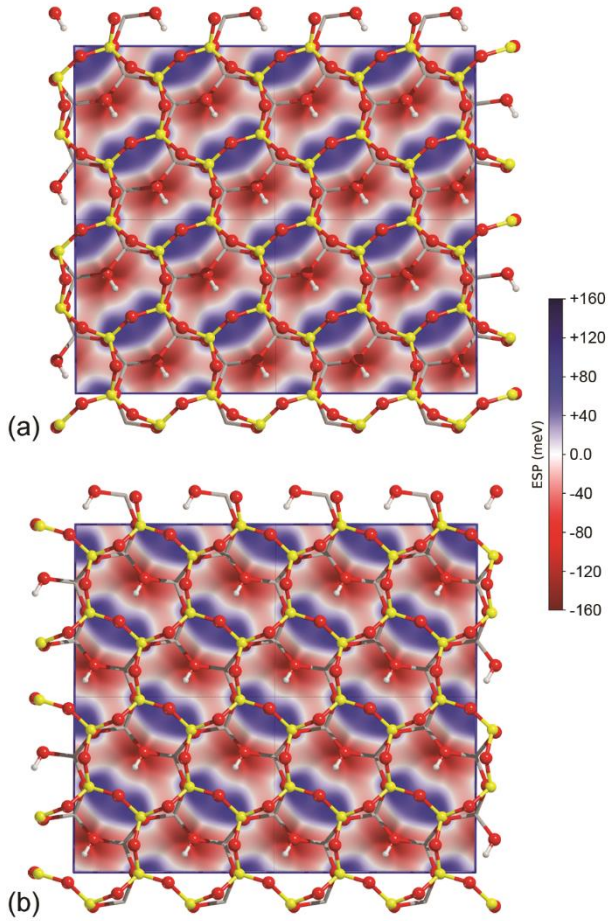

Figure 2. Three-dimensional electrostatic surface potential (ESP) maps of (**a**) top and (**b**) bottom faces of (001) slab model of pyrophyllite, superimposed by a ball-and-stick representation of the atoms exposed at the two surfaces. For the sake of clarity, a 2 × 2 repetition of the electrostatic surface potential is reported. Octahedrally-coordinated aluminium atoms are represented as a grey network. Colour code for atoms: Si – yellow, O – red, H – white.

The three-dimensional ESP maps typically find their usefulness in the identification of docking sites for molecular adsorbates, such as water, according to the principle of electrostatic complementarity. From this perspective, considering also the slab atoms exposed at the surface, one should expect the formation of O – H --- O(b) long-range interactions (H-bonds) between the hydrogen atoms of the molecule and the basal oxygen of the silicate tetrahedra. However, this naïve hypothesis has to be verified by geometrical optimization of the (001) PYP slab/water system.

3.2. Water adsorption from static simulations

To model the interaction of water with the layered silicate, a single H_2O molecule (W1) was placed on the surface of the (001) PYP slab, naming this model as PYP-W1. In the following, O and H atoms of water were identified by O_W and H_W labels, respectively. The adsorbate was placed with its plane parallel to the surface and at a distance of 4 Å from the latter. Then, the PYP-W1 model system was geometrically optimized within the *P*1 space group, in other words no symmetry operation constrained the relaxation procedure. In addition to the starting distance between water and the surface, this operation required several optimization steps (ca. 70). However, this approach is preferred over placing the molecule near a possible docking site (*i.e.* fewer optimization cycles required) because the adsorbant is free to roto-translate (movements in the three-dimensional space) and deform (variation of O_W – H_W lengths and H_W – O_W – H_W angle) to find the best adsorption conformation.

A graphical representation of the optimized PYP-W1 model is shown in Figures 3a,b, whereas the binding and other energy contributions are reported in Table 3. On this neutral 2:1 phyllosilicate, E_B^C is negative (ca. –17 kJ mol^{-1}), but the electronic contribution (*i.e.*, excluding that from the dispersive forces) turned to be positive (+0.15 kJ mol^{-1}). The water molecule interacts with the basal oxygen atoms at a distance of about 2.21 Å, which is greater than the typical threshold for hydrogen bond formation (2.1 Å). The H_2O plane is canted with respect to the surface by about 50°, with the oxygen atom repelled by the negative potential exerted by the underneath O(h) atom of the slab, as suggested from the electrostatic surface potential maps previously discussed. Conversely, in the work of Moro et al. (2020a), a water molecule on a single (001) layer of talc was adsorbed with the molecular plane almost parallel to the slab surface, exhibiting a long-range interaction between the O_W and the hydrogen of the underneath hydroxyl group, as graphically reported in Figure S1 (Supplementary Materials). All these results suggest a very low interaction between the molecule and the pyrophyllite surface. As further evidence, both water and (001) surface show a very low (less than 2 kJ mol^{-1}) deformation energy, ΔE_W, and δE_S, respectively. The observed geometrical conformations of a single water molecule interacting with the different stoichiometric (001) phyllosilicate surfaces (pyrophyllite and talc) is useful for explaining their hydrophobicity/hydrophilicity and the related technological behaviours of the two minerals.

In addition, to investigate the effects of the weak van der Waals interaction in the adsorption of water onto the basal surface of pyrophyllite, the geometry optimization and binding energy analysis

were carried out without including any *a posteriori* correction for long-range interactions (B3LYP approach). The resulting H_2O molecular conformation is similar to that obtained from the B3LYP-D* method, but the H_W --- O(b) interactions occur at longer distances (about 2.36 Å), meaning that there is an increased repulsion between the adsorbate and the mineral surface. The calculated binding energy is negative, but its absolute value is very low (E_B^C = –2.10 kJ mol^{-1}, see Table 1). Hence, considering that DFT simulations are accompanied by uncertainties of at least 4 kJ mol^{-1} (see Hao et al., 2013), the electronic contribution to the adsorption energy calculated with the B3LYP-D* approach (+0.15 kJ/mol) and that obtained by completely neglecting the long-range interactions (B3LYP only) are comparable.

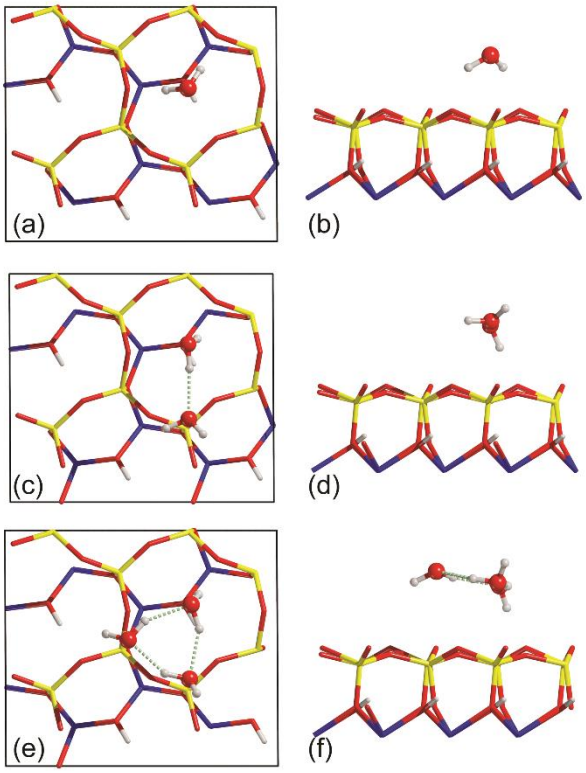

Figure 3. Unit cell views of the optimized models used to simulate the water adsorption on pyrophyllite: (**a**, **b**) PYP-W1, (**c**, **d**) PYP-W2, and (**e**, **f**) PYP-W3. The panels on the left are views of the systems along the [001] direction, whereas those on the right are related to views along the [100] direction. The water molecule and the (001) slab were represented as a ball-and-stick model and as a wireframe, respectively. Light green dashed lines are hydrogen bonds. Colour code for atoms: Si – yellow, Al – blue, O – red, H – white.

To model the increase of the (001) surface hydration layer, a second water molecule was placed at about 4 Å from the surface of the previous PYP-W1, with the H_2O plane parallel to the slab. This new model was labelled PYP-W2, and the geometry optimization result is graphically shown in Figures 3c,d, whereas the normalized binding energy per water molecule is reported in Table 3.

Having left enough space for the free transformation (deformation, rotation, and translation) of each adsorbate on the slab surface during the optimization procedure, the PYP-W2 system shows a different conformation of water with respect to the single molecule case. In fact, there is a strong interaction between the two H_2O molecules, establishing a hydrogen bond and acquiring a conformation very similar to that of the water dimer in the gas phase. This is an interesting sign of weak engagement between the water system and the (001) surface, which is also evinced by the different contributions to the binding energy. The absolute E_B^C value of the PYP-W2 system is greater than that of PYP-W1, but this is artificially incremented by the H_2O --- H_2O interaction (ΔE_L^C = –12.82 kJ mol^{-1}). In this case, a better estimation of the water-to-slab interaction is given by the E_B^{*C} value that, by definition in Eq.(9), represents the BSSE-corrected binding energy between the water cluster and the slab. For pyrophyllite, E_B^{*C} is negative, but the electronic contribution is positive (+0.80 kJ mol^{-1}): this means there is an electrostatic repulsion between the two layers, which are held together by weak long-range interactions. As observed for the PYP-W1 system, only very small deformation energies for water (ΔE_W) and the slab (δE_S) were calculated. It is interesting to note also that δE_S (PYP-W2) ≈ 0.5 δE_S (PYP-W1), further highlighting the negligible effect of the water dimer on the deformation of the (001) slab.

The addition of the third water molecule on the (001) pyrophyllite surface resulted in further signs of self-assembly of the water molecules, a process that is preferred over water-to-slab interactions, as graphically shown in Figures 3e,f. In detail, the three H_2O create an almost triangular cluster, where each side is given by three atoms (O_W – H_W --- O_W). One water molecule is above the centre of the SiO_4 pseudo-hexagonal ring, whereas the other two molecules are each one above a silica tetrahedron, with the oxygen atom (negative potential) interacting with the silicon one (positive potential). The hydrogen bonds between the water molecules are established with a mean distance of 1.918 Å, and the mean distance between the oxygen atoms of H_2O (O_W – O_W) is 2.809 Å. As calculated for the other systems, also for PYP-W3 the E_B^{*C} is negative (–11.55 kJ mol^{-1}) but with repulsive electronic energy contribution (+0.32 kJ mol^{-1}).

Even in this case, the deformation energy is small for both the adsorbant and for the (001) pyrophyllite surface. However, it is interesting noting that (i) the water three molecules are more deformed by the single and the dimer cases, because of their reciprocal interactions and (ii) the δE_S for PYP-W3 falls between PYP-W1 and PYP-W2. For the latter, this result is due to the different length (and number) of the long-range H_W --- O(b) interaction(s): in the PYP-W3 system, there is a

single one at 2.165 Å, for PYP-W2 the length is the longest (2.237 Å) and for the PYP-W1 system the single water molecule established two interactions at 2.209 Å and 2.204 Å.

Table 3. Binding energies E_B^C (in kJ mol^{-1} per water molecule) calculated at the B3LYP-D* level of theory corrected for the basis set superposition error, together with the different energy contributions as a function of increasing coverage and (001) surface slab model (see Materials and Methods for details).

Model	δE_W	ΔE_W	ΔE_L	ΔE_L^C	δE_S	E_B^*	E_B^{*C}	E_B	E_B^C	BSSE
PYP-W1	0.47	0.01	0.46	0.46	1.25	–26.36	–18.92	–24.64	–17.19	7.44
PYP-W1 (no vdW)	0.43	0.01	0.42	0.42	0.86	–9.92	–3.39	–8.63	–2.10	6.54
PYP-W2	–12.74	0.08	–13.74	–12.82	0.68	–16.65	–11.80	–29.62	–25.69	3.93
PYP-W3	–23.76	0.65	–27.20	–24.41	0.95	–15.81	–11.55	–41.40	–34.59	6.82

Notes: PYP-W1 (no vdW) is related to energy term evaluated at the B3LYP level, without the correction for dispersive forces.

Due to the known hydrophobic behaviour of pyrophyllite, only few works considered the interaction between the (001) surface of PYP and water. The present results concerning the geometry and binding energy of a single water molecule are in line with those reported by Churakov (2006). The *ab initio* molecular dynamics simulations conducted at the PBE level of theory with Vanderbilt pseudopotentials showed an extremely low and positive binding energy (1 kJ mol^{-1} – 2 kJ mol^{-1}) for the water-(001) pyrophyllite surface interaction, which was lower than the water-water binding energy (Bridgeman et al., 1996). Albeit no correction for dispersive forces was employed by the author as it was not available at that time, this result agrees with the findings obtained at the DFT/B3LYP-D* level of theory for the electronic contribution to BE^C. The small differences between the PBE results of Churakov (2006) and those here calculated with the B3LYP hybrid functional (without correction for dispersive forces) is within the DFT uncertainties.

Zhang and co-workers (2012) performed a simulation of different water loadings on pyrophyllite, using the VASP code and the dispersion-corrected PBE-D2 approach. They find that for one, two, and three molecules the binding energy was about –13.9 kJ mol^{-1}, –40.5 kJ mol^{-1}, and –44.4 kJ mol^{-1}, respectively, which are in line with the present BE^C results. In addition, the most stable conformations are geometrically very close to those reported in this work, in particular the formation of the dimer and trimer triangular clusters. However, there is a small discrepancy between the binding energy obtained from the pure electronic contribution. In fact, Zhang et al. (2012) reported, only for the single molecule case, a small negative (meaning attraction) binding energy of about –1 kJ mol^{-1}. In the present work, for all the water coverages, the electronic BE^C was positive from +0.15 kJ mol^{-1} to 0.80 kJ mol^{-1}. Notwithstanding this very small difference (± 1 kJ mol^{-1}) that is within typical uncertainties at both experimental and DFT levels, it is clear from both

the present work and one of Zhang and co-workers (2012) that the adsorption of water on pyrophyllite is completely driven by long-range interactions.

Finally, with respect to adsorption of a single water molecule on talc [$Mg_3Si_4O_{10}(OH)_2$, the trioctahedral 2:1 phyllosilicate], whose E_B^C = –23.30 kJ mol^{-1} (Moro et al., 2020a), PYP has a lower interaction with water.

3.3. AIMD simulations of water adsorption

The starting model used to simulate the time evolution dynamic of water on (001) pyrophyllite was the PYP-W3 system. Differently from the static results at 0 K, where the code allowed simulating the surface as a 2D system, AIMD simulations with QuantumATK require a 3D periodic unit cell. Hence, the *a* and *b* lattice parameters were initially set as those calculated with CRYSTAL in static conditions, and the third dimension (*c* lattice parameter) was set to 20 Å to reduce the interaction between the slab and its replicas along the *z*-direction. After equilibration, the mean temperature and pressure recorded during the 5000 fs production runs were 306.52 K and –0.004 kbar, respectively.

In general, the dynamics of the adsorption of three water molecules on the (001) pyrophyllite surface showed the same triangular cluster configuration of the adsorbates, with two molecules above a SiO_4 tetrahedron each and the last one above the pseudo-hexagonal siloxane ring. This observation well agrees with the results obtained at 0 K (see Figures 3e,f). The radial distribution functions (RDFs) of atomic distances (with a cut-off radius of 5 Å, *i.e.*, the maximum sampled atomic distance, see Figure 4) provide further geometrical details on the dynamics of the adsorbate over the (001) layered silicate slab. There is a long-range O_W --- Si interaction with a first peak at 2 Å and a second one at about 4 Å, which are both due to the two water molecules placed over the SiO_4 tetrahedra. This is in line with the two long-range interactions at 3.12 Å and 3.57 Å found with the static simulations.

The RDF-related interaction of water through its hydrogen atoms with the surface basal oxygen, H_W --- O(b), shows a first broad peak at about 2.0 Å, in agreement with the typical length of a hydrogen bond. Its small intensity compared to the broad peak centred at about 3 Å shows that the molecules did not strongly interact with the (001) surface of pyrophyllite.

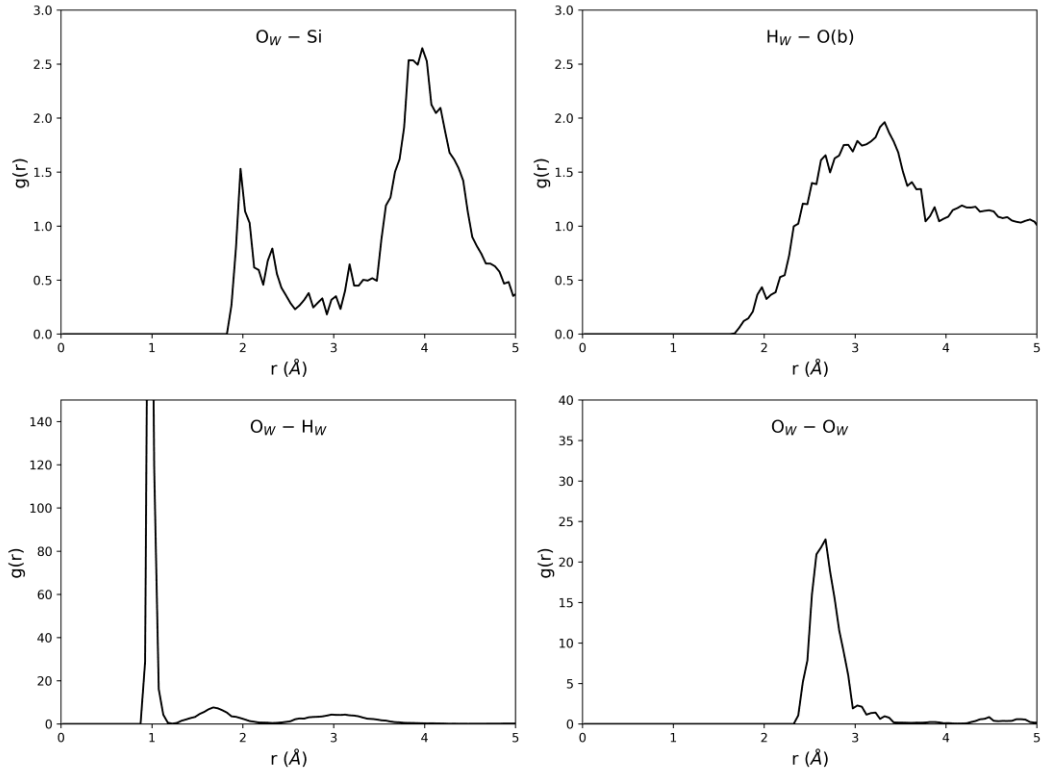

Figure 4. Radial distribution functions (RDFs) calculated for different atomic interactions: O_W – Si, H_W – O(b), O_W – H_W and O_W – O_W.

The O_W – H_W RDF shows a very sharp and intense peak centred at about 0.97 Å for each surface model, which is related to O – H covalent bonds within water molecules. Then, a second broader peak is centred at 1.68 Å: in this case, the calculated lengths are in line with those of typical hydrogen bonds in water clusters. The radial distribution function for the O_W – O_W interaction shows a single, slight broad peak centred at about 2.67 Å, in agreement with that calculated statically (2.81 Å). These shorter distances obtained with the PBE-D2 approach compared to that calculated at the DFT/B3LYP-D* level at 0 K could be due to (i) the different basis sets, (ii) an overbinding effect of the D2 correction for long-range interactions, other than the well-known differences between standard GGA functionals and hybrid ones.

The present AIMD results are in reasonable agreement with the previous molecular mechanics simulations conducted by Zhang and co-workers (2012) using the LAMMPS code (Plimpton, 1995) and CLAYFF force field for the mineral substrate (Cygan et al., 2004). In fact, the authors reported the cyclic H_2O trimer (labelled as 3a) being the most energetically stable configuration of the adsorbate on the (001) pyrophyllite surface. A second, chain-like configuration (3b) of the water trimer was found at molecular mechanics level, but it was found less stable than the cyclic cluster in an energy range between 3 kJ mol^{-1} and 10 kJ mol^{-1} according to the force field adopted for water,

either rigid SPC (Berendsen et al.), flexible SPC (Teleman et al., 1987) or TIP4P (Abascal and Vega, 2005). Throughout the AIMD simulation performed in the present paper, the 3b configuration described by Zhang et al. (2012) was not found. As also suggested by the cited authors, this difference could origin from the computational approach employed for modelling the water/mineral interaction. In fact, although the CLAYFF simulations were able to reproduce the binding energies of water molecules on the surface found in the PBE-D2 calculations, the force field approach resulted in much shorter hydrogen bond lengths and smaller values of the E_B values (Zhang et al., 2012). This could be related to the CLAYFF/SPC force field, and the present results could be useful for a future re-parametrization of the non-bonding interactions between water and the (001) surface of phyllosilicates.

4. Conclusions

In the present work, the adsorption behaviour of water onto the (001) surface of pyrophyllite was investigated in detail through *ab initio* simulations carried out in both static (0 K) and ambient (300 K, 1 bar) conditions. The (001) surface model considered a single TOT layer composed of only two tetrahedral sheets of SiO_4 groups that sandwich the octahedrally-coordinated Al cations. The results further demonstrated the hydrophobic nature of the (001) surface of pyrophyllite, as the binding energy for the water adsorption is small, and for increasing loadings the solvent prefers dimerizing (two molecules) or creating a triangular cluster (three molecules). These geometries are typical of gas-phase-like interaction between H_2O molecules, a clear indication of the hydrophobic nature of the substrate and higher water-water interactions, as also revealed by the lateral interaction contributions $\Delta E_L{}^C$. However, the present study showed the details of the geometrical relations between the molecules (single and self-assembled) and the mineral surface. The results here reported are in good agreement with other theoretical studies performed with different computational approaches, with and without corrections to include dispersive forces. The present data extend the knowledge on the hydration of the external surface of neutral 2:1 phyllosilicates at the quantum mechanical level, which could be of great use in applications and developments of this kind of minerals. For example, it could be devised the modulation of surface properties of pyrophyllite (or other phyllosilicates) to increase hydrophilicity or hydrophobicity by variation of the TOT crystal chemistry.

In addition, for large-scale modelling at the mesoscale it is mandatory relying on force fields because it is necessary to consider thousands of atoms in a simulation box. It is worth remembering

that force fields are usually general purpose for broad applications within a specific type of materials (organic/inorganic, solutions, minerals, biomolecules, and so on), but they are parametrized on experimental/quantum mechanical data obtained for these systems. The present data, obtained with *ab initio* static and molecular dynamics simulations, could be a good starting point to further develop refined force fields for the description of phyllosilicate-water adsorption/interaction processes. This would open further atomistic studies involving thousands of atoms, which will be closer to the real experimental samples. These fundamental *in silico* studies from the atomic level to the mesoscale could be employed to better understand the hydration of clay minerals, to drive applied research for desired rheological and technological properties, or the synthesis of hydrophobic clay/polymer composite films, just to cite some examples.

As a final note, the present work further shows the relevancy of the adoption of corrections or specifically developed functionals to include long-range interactions in the total DFT energy of a system. Indeed, this is not a trivial point when dealing with minerals and materials characterized by heterodesmic structures. Also, *ab initio* simulations with different levels of accuracies and settings (temperature, pressure, time-scale, etc.) can provide atomistic insights on surface properties and processes occurring on them, which could be of use in both understanding and predicting the behaviour of minerals/materials with tailored crystal-chemistry.

Funding: This research did not receive any specific grant from funding agencies in the public, commercial, or not-for-profit sectors.

Conflicts of interest: the authors declare no conflict of interest.

Availability of data: within the present article.

Author Contributions: Conceptualization, G.U., D.M. and G.V.; methodology, G.U.; validation, G.U., D.M. and G.V.; formal analysis, G.U.; investigation, G.U., D.M. and G.V.; data curation, G.U.; writing—review and editing, G.U., D.M. and G.V.; visualization, G.U.; supervision, G.V. All authors have read and agreed to the published version of the manuscript.

References

Abascal, J.L.F., Vega, C., 2005. A general purpose model for the condensed phases of water: TIP4P/2005. Journal of Chemical Physics 123.

Baranava, M., Hvazdouski, D., Stempitsky, V., Vauchok, S., Najbuk, M., 2018. Electronic and optic properties of transition metal dichalcogenides (MoS2, WSe2) and graphene heterostructures. Mater. Phys. Mech. 39, 8-14.

Becke, A.D., 1993. Density-Functional Thermochemistry .3. The Role of Exact Exchange. Journal of Chemical Physics 98, 5648-5652.

Berendsen, H.J.C., Grigera, J.R., Straatsma, T.P., 1987. The missing term in effective pair potentials. Journal of Physical Chemistry 91, 6269-6271.

Bhasin, S., Amritphale, S.S., Chandra, N., 2003. Effect of pyrophyllite additions on sintering characteristics of fly ash based ceramic wall tiles. British Ceramic Transactions 102, 83-86.

Boys, S.F., Bernardi, F., 1970. The calculation of small molecular interactions by the differences of separate total energies. Some procedures with reduced errors. Mol. Phys. 19, 553-566.

Bridgeman, C.H., Buckingham, A.D., Skipper, N.T., Payne, M.C., 1996. Ab-initio total energy study of uncharged 2:1 clays and their interaction with water. Mol. Phys. 89, 879-888.

Bruno, M., Prencipe, M., Valdrè, G., 2006. Ab initio quantum-mechanical modeling of pyrophyllite Al2Si4O10(OH)(2) and talc Mg3Si4O10(OH)(2) surfaces. Physics and Chemistry of Minerals 33, 63-71.

Catti, M., Valerio, G., Dovesi, R., Causa, M., 1994. Quantum-mechanical calculation of the solid-state equilibrium MgO + alpha-Al_2O_3 $MgAl_2O_4$ (spinel) versus pressure. Physical Review B 49, 14179-14187.

Cheng, J., Gao, L., Li, T., Mei, S., Wang, C., Wen, B., Huang, W., Li, C., Zheng, G., Wang, H., Zhang, H., 2020. Two-Dimensional Black Phosphorus Nanomaterials: Emerging Advances in Electrochemical Energy Storage Science. Nano-Micro Lett. 12.

Chiatti, F., Delle Piane, M., Ugliengo, P., Corno, M., 2016. Water at hydroxyapatite surfaces: the effect of coverage and surface termination as investigated by all-electron B3LYP-D* simulations. Theor Chem Acc 135.

Churakov, S.V., 2006. Ab initio study of sorption on pyrophyllite: Structure and acidity of the edge sites. Journal of Physical Chemistry B 110, 4135-4146.

Civalleri, B., Zicovich-Wilson, C.M., Valenzano, L., Ugliengo, P., 2008. B3LYP augmented with an empirical dispersion term (B3LYP-D*) as applied to molecular crystals. CrystEngComm 10, 405-410.

Corno, M., Busco, C., Bolis, V., Tosoni, S., Ugliengo, P., 2009. Water Adsorption on the Stoichiometric (001) and (010) Surfaces of Hydroxyapatite: A Periodic B3LYP Study. Langmuir 25, 2188-2198.

Cutini, M., Maschio, L., Ugliengo, P., 2020. Exfoliation Energy of Layered Materials by DFT-D: Beware of Dispersion! Journal of Chemical Theory and Computation 16, 5244-5252.

Cygan, R.T., Liang, J.J., Kalinichev, A.G., 2004. Molecular models of hydroxide, oxyhydroxide, and clay phases and the development of a general force field. Journal of Physical Chemistry B 108, 1255-1266.

Dong, H.M., Guo, S.D., Duan, Y.F., Huang, F., Xu, W., Zhang, J., 2018. Electronic and optical properties of single-layer MoS2. Front. Phys. 13, 6.

Dovesi, R., Erba, A., Orlando, R., Zicovich-Wilson, C.M., Civalleri, B., Maschio, L., Rerat, M., Casassa, S., Baima, J., Salustro, S., Kirtman, B., 2018. Quantum-mechanical condensed matter simulations with CRYSTAL. Wires Comput Mol Sci 8, E1360.

Evans, B.W., Guggenheim, S., 1988. Talc, Pyrophyllite, and Related Minerals. Rev. Mineral. 19, 225-294.

Fuchs, M., Scheffler, M., 1999. Ab initio pseudopotentials for electronic structure calculations of poly-atomic systems using density-functional theory. Comput Phys Commun 119, 67-98.

Gatti, C., Saunders, V.R., Roetti, C., 1994. Crystal-field effects on the topological properties of the electron-density in molecular-crystals - the case of urea. Journal of Chemical Physics 101, 10686-10696.

Grimme, S., 2006. Semiempirical GGA-type density functional constructed with a long-range dispersion correction. Journal of Computational Chemistry 27, 1787-1799.

Hao, P., Sun, J., Xiao, B., Ruzsinszky, A., Csonka, G.I., Tao, J., Glindmeyer, S., Perdew, J.P., 2013. Performance of meta-GGA Functionals on General Main Group Thermochemistry, Kinetics, and Noncovalent Interactions. Journal of Chemical Theory and Computation 9, 355-363.

Kwon, K.D., Newton, A.G., 2016. Structure and stability of pyrophyllite edge surfaces: Effect of temperature and water chemical potential. Geochim Cosmochim Ac 190, 100-114.

Lee, C.T., Yang, W.T., Parr, R.G., 1988. Development of the Colle-Salvetti Correlation-Energy Formula into a Functional of the Electron-Density. Physical Review B 37, 785-789.

Lee, J.H., Guggenheim, S., 1981. Single-crystal X-Ray refinement of pyrophyllite-1Tc. American Mineralogist 66, 350-357.

Mak, K.F., Lee, C., Hone, J., Shan, J., Heinz, T.F., 2010. Atomically thin MoS2: A new direct-gap semiconductor. Physical Review Letters 105.

Martyna, G.J., Klein, M.L., Tuckerman, M., 1992. Nose-Hoover chains: the canonical ensemble via continuous dynamics. Journal of Chemical Physics 97, 2635-2643.

Martyna, G.J., Tobias, D.J., Klein, M.L., 1994. Constant-Pressure Molecular-Dynamics Algorithms. Journal of Chemical Physics 101, 4177-4189.

Monkhorst, H.J., Pack, J.D., 1976. Special points for Brillouin-zone integrations. Physical Review B 8, 5188-5192.

Moro, D., Ulian, G., Valdre, G., 2019a. 3D meso-nanostructures in cleaved and nanolithographed Mg-Al-hydroxysilicate (clinochlore): Topology, crystal-chemistry, and surface properties. Applied Clay Science 169, 74-80.

Moro, D., Ulian, G., Valdrè, G., 2015. Single molecule investigation of glycine-chlorite interaction by cross-correlated scanning probe microscopy and quantum mechanics simulations. Langmuir : the ACS journal of surfaces and colloids 31, 4453-4463.

Moro, D., Ulian, G., Valdrè, G., 2019b. Amino acids-clay interaction at the nano-atomic scale: The L-alanine-chlorite system. Applied Clay Science 172, 28-39.

Moro, D., Ulian, G., Valdrè, G., 2020a. Nano-atomic scale hydrophobic/philic confinement of peptides on mineral surfaces by cross-correlated SPM and quantum mechanical DFT analysis. J. Microsc. 280, 204-221.

Moro, D., Ulian, G., Valdrè, G., 2020b. Nanoscale oligopeptide adsorption behaviour on chlorite as revealed by scanning probe microscopy and density functional simulations. Applied Clay Science 197.

Nada, R., Nicholas, J.B., McCarthy, M.I., Hess, A.C., 1996. Basis sets for ab initio periodic Hartree-Fock studies of zeolite/adsorbate interactions: He, Ne, and Ar in silica sodalite. International Journal of Quantum Chemistry 60, 809-820.

Novoselov, K.S., Geim, A.K., Morozov, S.V., Jiang, D., Zhang, Y., Dubonos, S.V., Grigorieva, I.V., Firsov, A.A., 2004. Electric field effect in atomically thin carbon films. Science 306, 666-669.

Pan, C.T., Nair, R.R., Bangert, U., Ramasse, Q., Jalil, R., Zan, R., Seabourne, C.R., Scott, A.J., 2012. Nanoscale electron diffraction and plasmon spectroscopy of single- and few-layer boron nitride. Physical Review B 85, 7.

Pawley, A.R., Clark, S.M., Chinnery, N.J., 2002. Equation of state measurements of chlorite, pyrophyllite, and talc. American Mineralogist 87, 1172-1182.

Perdew, J.P., Burke, K., Ernzerhof, M., 1996. Generalized gradient approximation made simple. Physical Review Letters 77, 3865-3868.

Plimpton, S., 1995. Fast parallel algorithms for short-range molecular dynamics. J. Comput. Phys. 117, 1-19.

Quaranta, E., Mesto, E., Lacalamita, M., Malitesta, C., Mazzotta, E., Scelsi, E., Schingaro, E., 2021. Using a natural chlorite as catalyst in chemical recycling of waste plastics: Hydrolytic depolymerization of poly-[bisphenol A carbonate] promoted by clinochlore. Waste Manage 120, 642-649.

Schlegel, H.B., 1982. Optimization of equilibrium geometries and transition structures. Journal of Computational Chemistry 3, 214-218.

Smidstrup, S., Markussen, T., Vancraeyveld, P., Wellendorff, J., Schneider, J., Gunst, T., Verstichel, B., Stradi, D., Khomyakov, P.A., Vej-Hansen, U.G., Lee, M.E., Chill, S.T., Rasmussen, F., Penazzi, G., Corsetti, F., Ojanperä, A., Jensen, K., Palsgaard, M.L.N., Martinez, U., Blom, A., Brandbyge, M., Stokbro, K., 2020. QuantumATK: An integrated platform of electronic and atomic-scale modelling tools. Journal of Physics Condensed Matter 32, 015901.

Smidstrup, S., Stradi, D., Wellendorff, J., Khomyakov, P.A., Vej-Hansen, U.G., Lee, M.E., Ghosh, T., Jonsson, E., Jonsson, H., Stokbro, K., 2017. First-principles Green's-function method for surface calculations: A pseudopotential localized basis set approach. Physical Review B 96.

Teleman, O., Jönsson, B., Engström, S., 1987. A molecular dynamics simulation of a water model with intramolecular degrees of freedom. Mol. Phys. 60, 193-203.

Tunega, D., Bucko, T., Zaoui, A., 2012. Assessment of ten DFT methods in predicting structures of sheet silicates: Importance of dispersion corrections. Journal of Chemical Physics 137.

Ulian, G., Moro, D., Valdrè, G., 2018. First principle investigation of the mechanical properties of natural layered nanocomposite: Clinochlore as a model system for heterodesmic structures. Compos. Struct. 202, 551-558.

Ulian, G., Moro, D., Valdrè, G., 2020. Infrared and Raman spectroscopic features of clinochlore Mg6Si4O10(OH)8: A density functional theory contribution. Applied Clay Science 197.

Ulian, G., Moro, D., Valdrè, G., 2021. Electronic and optical properties of graphene/molybdenite bilayer composite. Compos. Struct. 255.

Ulian, G., Tosoni, S., Valdrè, G., 2013. Comparison between Gaussian-type orbitals and plane wave ab initio density functional theory modeling of layer silicates: Talc $Mg_3Si_4O_{10}(OH)_2$ as model system. Journal of Chemical Physics 139.

Ulian, G., Tosoni, S., Valdrè, G., 2014. The compressional behaviour and the mechanical properties of talc [$Mg_3Si_4O_{10}(OH)_2$]: a density functional theory investigation. Physics and Chemistry of Minerals 41, 639-650.

Ulian, G., Valdrè, G., 2015a. Density functional investigation of the thermo-physical and thermo-chemical properties of 2M(1) muscovite. American Mineralogist 100, 935-944.

Ulian, G., Valdrè, G., 2015b. Density functional investigation of the thermophysical and thermochemical properties of talc Mg3Si4O10(OH)(2). Physics and Chemistry of Minerals 42, 151-162.

Ulian, G., Valdrè, G., 2015c. Structural, vibrational and thermophysical properties of pyrophyllite by semi-empirical density functional modelling. Physics and Chemistry of Minerals 42, 609-627.

Ulian, G., Valdrè, G., 2019. Equation of state and second-order elastic constants of portlandite $Ca(OH)_2$ and brucite $Mg(OH)_2$. Physics and Chemistry of Minerals 46, 101-117.

Valdrè, G., Moro, D., Ulian, G., 2011. Nucleotides, RNA and DNA selective adsorption on atomic-flat Mg-Al-hydroxysilicate substrates. Micro & Nano Letters 6, 922-926.

Valenzano, L., Torres, F.J., Klaus, D., Pascale, F., Zicovich-Wilson, C.M., Dovesi, R., 2006. Ab initio study of the vibrational spectrum and related properties of crystalline compounds; the case of $CaCO_3$ calcite. Z Phys Chem 220, 893-912.

Yang, J., Tang, L.S., Bao, R.Y., Bai, L., Liu, Z.Y., Xie, B.H., Yang, M.B., Yang, W., 2018. Hybrid network structure of boron nitride and graphene oxide in shape-stabilized composite phase change materials with enhanced thermal conductivity and light-to-electric energy conversion capability. Sol. Energy Mater. Sol. Cells 174, 56-64.

Zhang, G., Al-Saidi, W.A., Myshakin, E.M., Jordan, K.D., 2012. Dispersion-corrected density functional theory and classical force field calculations of water loading on a pyrophyllite(001) surface. Journal of Physical Chemistry C 116, 17134-17141.